In vivo resorption of injectable apatitic calcium phosphate cements: Critical role of the intergranular microstructure

Myriam Le Ferrec, Charlotte Mellier, François-Xavier Lefèvre, Florian Boukhechba, Pascal Janvier, Gilles F Montavon, Jean-Michel Bouler, Olivier Gauthier, Bruno Bujoli

In vivo resorption of injectable apatitic calcium phosphate cements (CPCs): critical role of the intergranular microstructure.

M. Le Ferrec,[a,b] C. Mellier,[a] F.-X Lefèvre,[c] F. Boukhechba,[a] P. Janvier,[c] G. Montavon,[b] J-M. Bouler,*[c] O. Gauthier,[d,e] and B. Bujoli*[c]

[a]Graftys SA, Eiffel Park, Bâtiment D, 415 Rue Claude Nicolas Ledoux, Pôle d'activités d'Aix en Provence, 13854 Aix en Provence CEDEX 3, (France), [b]SUBATECH, UMR CNRS 6457, IMT Atlantique Bretagne-Pays de la Loire, 4 rue Alfred Kastler, CS 20722, 44307 Nantes Cedex 03, (France), [c]Université de Nantes, CNRS, UMR 6230, CEISAM, UFR Sciences et Techniques, 2, rue de la Houssinière, BP 92208, 44322 NANTES Cedex 3 (France), [d]Université de Nantes, INSERM, UMR 1229, RMeS, Faculté de Chirurgie Dentaire, BP 84215, 44042 Nantes Cedex 1, (France), [e]ONIRIS, Nantes Atlantic College of Veterinary Medicine, Food Science and Engineering, Atlanpole-La Chantrerie, CS 40706, 44307 Nantes cedex 3, (France)

Email: bruno.bujoli@univ-nantes.fr

Abstract

The *in vivo* resorption rate of two injectable apatitic calcium phosphate cements used in clinics (Graftys® HBS and NORIAN®) was compared, using a GLP study based on an animal model of critical-sized bone defect. To rationalize the markedly different biological properties observed for both cements, key physical features were investigated, including permeability and water-accessible porosity, total porosity measured by mercury intrusion and gravimetry, and microstructure. Due to a different concept for creating porosity between the two cements investigated in this study, a markedly different microstructural arrangement of apatite crystals was observed in the intergranular space, which was found to significantly influence both the mechanical strength and *in vivo* degradation of the two CPCs.

Key words*: apatitic cement; polysaccharide; permeability; in vivo response; microstructure.*

1. Introduction

Since first reports made in the 1980s,[1-3] calcium phosphate cements (CPCs) have attracted significant interest as bone substitutes in trauma surgery.[4-7] Owing to their excellent biocompatibility, bioactivity and osteoconductivity, they can indeed be transformed into new bone by the cellular action of bone cells (osteoclasts and osteoblasts) responsible for the local bone remodeling. Unlike calcium phosphate bioceramics in granules or pre-shaped form, the ability of injectable CPCs to readily adapt to the shape of any bone defect and provide an intimate contact with the bone structure, is a major advantage.[8-12]

However, purely inorganic CPCs have most often critical drawbacks which limit their potential clinical application, including (*i*) a poor injectability which is usually characterized by filter-pressing[13-16] (*i.e.* a phase separation between the liquid and solid); (*ii*) a weak cohesion which results in the disintegration of the cement paste upon early contact with biological fluids[17,18]; (*iii*) mechanical properties not adapted for load-bearing conditions (*i.e.* low fracture toughness)[19-22]; (*iv*) insufficient porosity especially in the macro range (100-800µm), needed for optimal cell colonization that will favour both cement resorption and new bone formation[23-25].

Therefore many polymer additives (e.g. sodium alginate, hyaluronic acid, collagen, polypeptides, chitosan, cellulose ethers…)[26-43] have been admixed either to the powder or to the liquid phase of the CPC with the aim of improving their handling and / or mechanical properties. Among these additives, cellulose ethers, such as hydroxypropyl methyl cellulose (HPMC), are water-soluble derivatives of cellulose, which is the most abundant polymer in nature. They have been widely used as anti-washout admixtures in civil engineering to improve the cohesion and anti-washout performance of cement-based materials (i.e. Portland cement).[44-

[46] Furthermore, these versatile cellulose ethers are of current use in pharmacology for controlled drug release systems,[47,48] thanks to their biocompatible and biodegradable character that has been extensively documented.[49,50]

In a recent study,[31] we have demonstrated that the addition of a small amount of cellulose ether (*ca*. 1-2 wt.%) in the liquid phase of a cement made of α-tricalcium phosphate (α-TCP, 98 wt.%) and calcium deficient apatite (CDA, 2 wt.%), dramatically improved the injectability, cohesion and washout resistance of the resulting cement paste, with no detrimental effect on both the setting time and compressive strength. In this context, we have developed HPMC-containing apatitic CPC formulations that led to the commercialization of injectable products that benefit from 8 years of clinical experience and have proven efficiency in traumatology.[51-54] More recently, molecular species have been successfully combined to these commercially available injectable CPCs, to open the way to new indications. This includes for example (*i*) bupivacaine for the design of a CPC capable to locally deliver an anaesthetic drug for pain release[55]; (*ii*) iobitridol, a water-soluble iodinated aromatic contrast agent, for the design of an injectable radiopaque CPC suitable for image-guided implantation[56]. For both formulations, molded blocks of the corresponding CPC were immerged in a 0.9 wt.% sodium chloride solution at 37°C under static conditions, to simulate the release of bupivacaine (resp. iobitridol) from the cement paste under bone implantation conditions. Interestingly, up to ca.70% (resp. 80%) of the bupivacaine (resp. iobitridol) dose loaded in the CPC was found to be released in a time period of one week, showing that the entrapped molecules can easily diffuse out of the cement. This means that the permeability / porosity of the hardened cement is important enough to allow exchanges between the cement and the external liquid medium.

The aim of the present study is to investigate whether the presence of the cellulose ether (HPMC) present in the CPC composition plays a significant role on its permeability and porosity. Therefore, measurement of these two parameters was performed on the Graftys® HBS

[abbreviated as HBS] composition and its HPMC-free analogue [abbreviated as HBS-0]. For comparison, another purely inorganic commercially available CPC was also included in this study, i.e. NORIAN SRS® [abbreviated as NORIAN]. For that purpose different methods were used, including (*i*) permeability measurements based upon percolation of water through CPC blocks molded into a glass column (*ii*) water-accessible porosity measurements using tritiated water (HTO) (*iii*) porosity assessment by mercury intrusion and gravimetry (*iv*) SEM observations of polished cross-sections of the samples to investigate their microstructure. Finally, the *in vivo* behavior of the two commercial formulations (HBS and NORIAN) was compared via a GLP study where the two CPCs were implanted in rabbit femoral critical-sized bone defects. A significant difference in the remodeling process taking place between the two bone void fillers was thus observed, suggesting that although the cement porosity is indeed an important feature, the intergranular microstructure is a critical factor which influences the kinetics of the *in vivo* replacement of apatitic CPCs by newly formed bone.

2. Materials and methods

2.1 Calcium phosphate cement formulations

Three apatitic calcium phosphate cements (CPCs) were used in this study:

- Graftys® HBS [abbreviated as HBS], obtained from Graftys SA (Aix-en-Provence, France), is a mixture of 78 wt.% α-tricalcium phosphate (α-TCP) ($Ca_3(PO_4)_2$), 5 wt.% dicalcium phosphate dihydrate (DCPD) ($CaHPO_4$, $2H_2O$), 5 wt.% monocalcium phosphate monohydrate (MCPM) ($Ca(H_2PO_4)_2$, H_2O), 10 wt.% calcium-deficient hydroxyapatite (CDA) ($Ca_{10-x}[\ ]_x(HPO_4)y(PO_4)_{6-y}(OH)_{2-z}[\ ]_z$), 2 wt.% hydroxypropyl methyl cellulose (HPMC). The liquid phase consists of a 5 wt. % Na_2HPO_4 aqueous solution (liquid/powder ratio = 0.5 $mL.g^{-1}$).

- An HPMC-free analogue of Graftys® HBS [abbreviated as HBS-0] was especially prepared for this study, under the same conditions except that no HPMC was added to the fabrication

process.

- NORIAN SRS® [abbreviated as NORIAN], obtained from Synthes, is a mixture of 85 wt.% α-TCP, 12 wt.% calcium carbonate ($CaCO_3$), 3 wt.% MCPM. The liquid phase consists of a Na_2HPO_4 solution (liquid/powder ratio = ca. 0.5 $mL.g^{-1}$).

HBS and HBS-0 cement samples were prepared by mixing 8 g of the powdered preparation with their liquid phase for 2 min to ensure the homogeneity of the resulting paste before use. NORIAN cement samples were prepared according to the users' guide by means of the Synthes Rotary mixture. To investigate the properties of the hardened cements (mechanical strength, porosity, FTIR and XRD analyses), specimens of cylindrical shape (6mm in diameter and 12mm of length) were prepared by pressing the resulting pastes into Teflon molds using a spatula. The molds containing the paste were immersed in a saline solution (0.9 wt.% sodium chloride aqueous solution), then incubated in a homothermal oven at 37 °C for 72 hours, before being polished to obtain flat and parallel faces for the bulk specimens, that were then unmolded.

2.2 Methods

2.2.1. SEM experiments

The measurements were carried out on the samples used for the permeability measurements (see section 2.3). Then, a 1 mm^2 polished cross-section of the samples was obtained using a JEOL cross section polisher SM09010, by applying an argon ion beam accelerated by a voltage up to 6 kV perpendicular to the surface of each specimen for 6 hours. SEM observation of those samples were performed using a Field Emission Gun Scanning Electron Microscope (Jeol 7600F). Images were acquired on a back scattered electron mode with a 9 pA beam current and a 10 kV accelerated voltage.

2.2.2. Compressive strength measurements

The measurements were carried out on cylinder-shaped moulded samples under wet conditions, *i.e.* immediately after taking the specimens out of the hardening solution (see section 2.1). A

TAHD+ texture analyzer was used and the samples were submitted to increasing compression load (displacement of the compressive rig: 1 $mm.s^{-1}$), the profile of which was recorded until fracture. For each sample, six cylinders were used to calculate the mean and standard deviation (SD).

2.2.3. Porosity measurements

Cylinder-shaped moulded samples (see section 2.1) that were dried at 37°C (until there was no mass variation: *ca.* 3 days) were used to determine the porosity through gravimetry, according to the following equation: Porosity = 1- (ρ_{app} / ρ), where ρ_{app} stands for the apparent density of the CPC samples, measured by dividing their weight by their volume, and ρ stands for the density of samples measured by helium pycnometry. For each sample, six cylinders were used to calculate the mean and standard deviation (SD).

Porosimetry measurements by mercury intrusion were performed using an Autopore IV 950 apparatus (Micromeritics, Atlanta, GA) for a 0.4 to 30000 psia pressure range (0 to 2068 bars). For each cement (HBS, HBS-0 and NORIAN), the measurements were repeated on 5 samples, to obtain the total porosity and the pore entrance size distribution curve.

2.2.4. XRD and FTIR characterization

Cylinder-shaped moulded samples (see section 2.1), that were dried at 37°C for 72 hours, were then manually crushed to a fine powder in an agate mortar for XRD and FTIR analysis. The XRD patterns were recorded by step scanning using a microprocessor-controlled diffractometer system, (Philips PW 1830 generator equipped with a vertical PW 1050 (y/2y) Goniometer and a PW 1711 Xe detector; Eindhoven, The Netherlands) with Ni-filtered copper Kα generated at 40 kV and 30 mA. The diffraction angle 2θ was varied from 5° to 70° by steps of 0.03° with a collection time of 2.3 sec per step.

The infrared data were registered with a Nicolet Magna II 550 Fourier transform infrared spectrometer (4 cm^{-1} resolution and 128 cumulated scans). The samples were pressed in KBr

pellets. The spectra were automatically baseline corrected by the OMNIC software package (Omnic 7.1, Thermo Electron Corporation, Madison, USA).

2.3 Permeability and water accessible porosity measurement

A glass column fitted with a PE filter was filled with a weighed quantity (see Table 1) of cement paste (HBS, HBS-0 or NORIAN). The CPCs were allowed to set for 7 days at 37°C in a humid chamber, by immersing the entire column in a 0.9 wt.% sodium chloride aqueous solution (NaCl), which was replaced every 2-3 days. The permeability (K) of the cement samples was determined by percolation of a 0.9 wt.% sodium chloride aqueous solution (NaCl), and the pressure gradient (dP) was measured as a function of the applied flow rate (dQ) following the Darcy law: $K = (dQ/dP) \times (L/S)$, where L and S correspond to the length and section of each cement block, respectively. The flow rate was adjusted using a high pressure pump (Gilson 307) and controlled at the column outlet by weighing aliquots of the solution. In the particular case of the HBS-0 cement which was found to be poorly permeable, application of a pressure at the column inlet was necessary to allow percolation of the liquid through the sample, and the flow rates were measured as a function of the applied pressure.

The water accessible porosity of the cement samples were determined by injection of tritiated water (HTO) (Cerca-Framatome), which was percolated through the columns under a 0.9 wt.% sodium chloride aqueous solution flow. 1000 Bq of HTO were injected and the elution profile was determined by analyzing ^{3}H in fractions of the eluted solution by liquid scintillation counting, using a Packard Tri-Carb 3170 TR/SL Liquid Scintillation analyzer. The scintillation cocktail was Ultima Gold LLT™ (Perkin Elmer). The water-accessible porosity was calculated as $(Vmax - Vd) \times 100 / Vc$, where Vmax is the eluted volume at the maximum of the ^{3}H detection (similar to the retention volume in liquid chromatography – see Figure S1 in Supporting Information), Vd is the dead volume of the column, and Vc is the volume of the

cement sample. In the case of the HBS-0 sample, the water accessible porosity was measured under controlled pressure (40 bars).

2.4 *In vivo study*

2.4.1. Animals and surgical procedures

The GLP study protocol (N° 137056) was submitted and approved by the Biomatech-Namsa Ethical Committee. Animal care and handling were performed in accordance with French animal welfare legislation. Animals manifesting one or more of the following criteria were scheduled for early removal following veterinarian advice: loss of more than 20% of initial body weight, inability to eat or drink, tumors of such size that they interfere with locomotion, ulceration of tumors or moribund animals. The tested biomaterials were implanted bilaterally for 4, 8 and 12 weeks at the distal end of 15 mature female New Zealand White rabbit femurs. Briefly, a lateral arthrotomy of the knee joint was performed and a cylindrical 6 x10 mm osseous critical-sized defect was created at the distal femoral end. After saline irrigation, the osseous cavity was carefully dried and filled with the tested cements. Each of the 15 rabbits was implanted with the HBS cement on one side and with the NORIAN one on the contra-lateral limb. At 4 weeks, 8 weeks and 12 weeks post implantation, five rabbits were euthanized and the implanted sites were sampled (n = 5 samples per cement and per time period).

2.4.2. Histological and histomorphometrical studies

For each time period, the distal femoral bone ends were dissected from their soft tissue attachments and classically prepared for histological examination on scanning and light microscopy. The femoral ends were fixed in a glutaraldehyde solution and successively dehydrated in graded ethanol and acetone. Eventually the non-decalcified bone specimens were infiltrated and embedded in a polymethylmethacrylate resin. The resulting resin blocks were cut in two halves perpendicular to the defect axis, providing two samples, one for light

microscopy histology and histomorphometry, one for SEM imaging. For light microscopy, undecalcified serial 7 mm sections of each sample were cut perpendicularly to the drilling axis of the implantation area using a hard tissue microtome (Reichert-Jung Supercut 2050, Austria), and stained with a modified Paragon polychromatic stain.

For SEM observations, the implant surface was polished and then sputtered with a thin layer of gold-palladium (EM Scope, England). SEM micrographs were taken using backscattered electrons at 15 kV and a ×50 magnification (Leo 1450VP, Zeiss, Germany). Images were acquired on the back-scattered electron mode, and areas of newly-formed mineralized bone, cements and non-mineralized tissue, respectively, were identified by their grey levels.

2.4.2. Histomorphometrical analysis of the implanted sites

The stained sections were used for the quantitative histomorphometrical evaluation conducted by scanning and slides were examined with a Zeiss Axioscope microscope (×5, ×10, ×25 and ×40 magnifications) equipped with a color images analyzing system (Samba®, version 4.27, SAMBA TECHNOLOGIES).

Two different concentric regions of interest (ROI) were defined (Figure 1): (i) standardized ROI 1 consisted of an approximately 1 mm thick circumferential layer around the implanted defect at the interface between the cement and the surrounding host bone, allowing quantitative measurements of superficial bone ingrowth and cement resorption at the bone tissue/cement interface. This peripheral ROI 1 approximately included the outer 500 µm of the implant and the first 500 µm of the surrounding host tissues; (ii) standardized ROI 2, consisted of a 5 mm in diameter circular area that included the inner core of the cement implant. In this area the deeper remodelling process was investigated within the implanted defect, allowing the quantitative measurement of bone ingrowth inside the implanted defect.

The quantitative histomorphometrical analysis was performed to assess and compare the percentages of the following parameters within ROI 1 and ROI 2, at the different implantation

times: (i) in ROI 1, the bone-to-cement contact or bone contact, i.e. the percentage of the cement perimeter in direct contact with mineralized bone tissue, corresponding to the peripheral osteointegration of the HBS and NORIAN cements; (ii) in ROI 1 and 2, the bone area density, as defined by the percentage of the ROI occupied by bone tissue in terms of surface area, and the cement area density, as defined by the percentage of the ROI occupied by the cement in terms of surface area.

Data were expressed as the means ± standard deviation (SD) and were compared between the two implanted cements, at the different implantation times. Statistical analysis of the histomorphometrical data was performed using a non-parametric Mann & Whitney test (Software SPSS® version 19.0, edited by SPSS Inc, Chicago, USA). P values < 0.05 were considered significant.

3. Results

3.1 Investigation of the permeability and water accessible porosity

The permeability and water-accessible porosity of the cement samples were determined by percolation of a 0.9 wt.% sodium chloride aqueous solution and tritiated water (HTO, as a conservative tracer for porosity) through glass columns filled with the selected cement paste (HBS, HBS-0 or NORIAN) that was allowed to set for 7 days at 37°C under humid conditions (see experimental section). As shown in Table 1, the porosity was also measured by mercury intrusion and gravimetry (ca 45-60%), and differential mercury intrusion curves (see Figure S2 in Supporting Information) showed the presence of (i) two main porosity domains for NORIAN: one is centered at 30 nm that corresponds to the intergranular space, and a larger one around 1 µm formed during the evacuation of CO_2 bubbles; (ii) three main porosity domains for HBS centered at 30, 115 and 650 nm, respectively. In this case, the 115 and 650 nm pores are very likely due to the presence of HPMC which is homogeneously distributed in the intergranular space and swells when preparing the cement paste. Interestingly, the HBS and

NORIAN compositions showed comparable permeability (ca 10^{-8} m s^{-1}). However, the very low values found for the water-accessible porosity (ca 5-9 %) are in sharp contrast with results obtained from mercury intrusion porosimetry. The situation with the HBS-0 cement was markedly different, since application of a 40 bars pressure at the column inlet was necessary to allow percolation of the liquid through the sample, as a result of a far lower permeability (ca 10^{-11} m s^{-1}). By contrast, the NORIAN composition which does not contain either any polymer additive, shows however a permeability very comparable to that of HBS.

3.2 Composition and characterization of the microstructure

The XRD patterns of the hardened HBS and NORIAN cements were identical, showing that these materials mainly consist of a poorly crystallized hydroxyapatite (Figure 2, top view). FTIR spectra (Figure 2, bottom view) were consistent with this result, showing however the formation of carbonated hydroxyapatite in the particular case of the NORIAN composition, in relation with the presence of calcium carbonate in this cement composition.

SEM observations of a fracture plane and polished cross-sections of the three samples were performed to compare their microstructure. In the case of the HBS and HBS-0 compositions, different types of particles can be observed: (i) a small amount of those are dense along their whole cross-section ("a" areas in Figure 3 – top views), that can be assigned to unreacted DCPA on the basis of the Ca/P ratio measured by Energy-dispersive X-ray spectroscopy (EDX); (ii) a large amount of particles have a geode-like morphology with a dense shell lined in its inner part with interdigitated platelet crystals, assigned to α-TCP particles fully hydrolyzed into CDA ("b" areas in Figure 3 – top views). The area in between all these particles is mostly occupied by a network of interdigitated platelet-like CDA crystals. It is important to note that occupation of the intergranular space by these interdigitated platelet-like CDA crystals is rather uniform for the HBS-0 composition, i.e. in the absence of the HPMC polymer in the formulation (see

Figure 3 – middle and bottom views). By contrast, for the HBS CPC, many voids are present in the intergranular space, in which no apatite formation occurred (see arrows in Figure 3 – middle and bottom views).

Interestingly, the microstructure of the NORIAN sample is significantly different. The SEM image of a fracture plane shows the presence of hollow ovoid-shaped particles in the 1-5 μm range (see Figure 4 – bottom view) corresponding to α-TCP particles fully transformed into apatite. On SEM images of a polished cross-section of the sample (see Figure 4 – top views), the space between these particles is mostly occupied by highly entangled tiny apatite needles, although a little amount of small voids are also present (see arrows on the Figure).

3.3 Compared *in vivo* behavior of HBS versus NORIAN

The HBS and NORIAN cements were implanted bilaterally at the distal end of mature female New Zealand White rabbit femurs. Each animal was implanted with the HBS cement on one side and with the NORIAN one on the contra-lateral limb. All animals recovered from surgery without any complication and all implantation sites healed uneventfully. Macroscopically, no local adverse effects were observed with the HBS and NORIAN cements after 4, 8 and 12 weeks of implantation. Histopathologically, HBS induced very slightly more local inflammation and irritation than NORIAN. This local inflammation was believed to be a transient event most likely related to the material degradation process that was significantly faster for HBS, as shown by the implant area density.

For both biomaterials, new bone growth was observed on the surface of the injected cement and progressed from the periphery towards the core of the defects. Mineralized mature bone was observed in close contact with the cements surface and between the degraded particles of the cements, without any fibrous interface.

In ROI 1, the bone-to-cement contact increased for both cements from 4 to 12 weeks after implantation. However no significant difference was present between the two groups. A progressive and significant degradation of the HBS cement was noted when increasing the implantation time (4, 8 and 12 weeks). NORIAN only showed a significant degradation between the fourth and twelfth week of implantation. The peripheral bone area density did not differ significantly between the two cements.

In ROI 2, the HBS cement always showed significantly more abundant new bone colonization that the NORIAN cement whatever the implantation time (Table 2). In addition, HBS showed a significantly more important degradation than NORIAN, 8 and 12 weeks after implantation (Figure 5).

4. Discussion

The objective of this study was to investigate in which extent the porosity and permeability of injectable apatitic cements are key factors in their ability to be rapidly resorbed *in vivo*. For that purpose, two commercially available CPCs were selected, for which the conception to make them porous was significantly different. In fact, the two cements showed comparable permeability (in the 10^{-8} m s^{-1} range), measured by percolation of a 0.9 wt.% sodium chloride aqueous solution and tritriated water through hardened cement blocks. Moreover, the sharp difference observed between the water-accessible porosity (ca 5-9 %) and the porosity measured by mercury intrusion (ca 45-60%), clearly suggested the presence of preferential paths when flowing a solution through the hardened cement samples. In the case of NORIAN which is a fast-setting cement (initial setting time: 4 min), as shown in Figure 4, the intergranular space of this CPC is mainly occupied by a highly dense network of small interlocked carbonated-hydroxyapatite needles. In addition, some voids of micrometric size are distributed at some places, as a result of the formation of CO_2 bubbles thanks to the presence

of calcium carbonate in the formulation. These large pores which are visible from the mercury intrusion curves (Figure S2), explain the presence of the preferential paths observed in the permeability measurements. By contrast, in the case of HBS (initial setting time: 15 min), a cellulose-based component (HPMC) is present in the cement composition, since it markedly improves the injectability, cohesion and washout resistance of the cement paste.[31] Interestingly, when adding the liquid phase to prepare the cement paste, the HPMC component swells and the resulting hydrogel occupies part of the intergranular space, which is no more available for apatite precipitation. As a result, the mineral density of interlocked hydroxyapatite platelet-like crystals in the intergranular space is far less for HBS when compared to its HPMC-free analogue (HBS-0; initial setting time: 7.5 min), for which a more tightly packed arrangement of the hydroxyapatite crystals was observed (Figure 3). Therefore, thanks to the polymer, large pores are also present in HBS (see arrows in Figure 3), although smaller than for NORIAN (Figure S2), but more homogeneously distributed in the intergranular space. Interestingly, the HPMC-free analogue of HBS (HBS-0) has a significantly lower permeability (in the 10^{-11} m s^{-1} range), that can directly be assigned to the absence of the HPMC component which also leads to an increase of the cement density (see Table 1). As no preferential path was present in that case, application of a 40 bars pressure at the column inlet was necessary to allow percolation of the liquid through the sample, and the water-accessible porosity and the porosity measured by mercury intrusion were comparable.

Given the similar permeability values but different microstructure observed for NORIAN and HBS, it was therefore interesting to investigate their compared *in vivo* degradation rate when implanted in bone sites. Hence, the two CPCs were implanted in critical-sized defects created in the distal lateral femoral condyle of rabbits, and HBS showed significantly higher bone substitution properties than NORIAN. This was confirmed by the quantitative histomorphometrical analysis, with a significantly higher bone area density at all implantation

times, as well as a significantly lower cement area density after 8 and 12 weeks of implantation (Table 2 and Figure 5). This is in full agreement with the histological images (see Figure S3) showing that the specific microstructure of HBS generates a diffused interface with the newly formed bone tissue, giving evidence of a more dynamic remodeling process than the one observed at the interface with the Norian cement. In summary, the HBS cement showed faster osteoconduction and material degradation than the NORIAN cement at all implantation times. In our opinion, this difference might be assigned to the intergranular microstructure which differs for the two hardened cements. While NORIAN and HBS have a similar water-accessible porosity (ca. 9 and 4.9 %, respectively) which allows percolation of the body fluids in the inner part of the cement implant, the arrangement of apatite in the intergranular space for NORIAN consists of very dense areas (made of small-sized tightly packed needles) which are separated by channels created by the evolution of carbon dioxide. By contrast, in the case of HBS, the porosity mediated by the polymer is homogeneously distributed in the intergranular space and the package density of the platelet-like apatite crystals is far lower when compared to NORIAN. This difference in the microstructure of the HBS and NORIAN hardened cements was also fully consistent with their respective compressive strength after a setting time of 24 hours which was more than twice higher for NORIAN (33±3 MPa) when compared to HBS (13±3 MPa). Likewise, the density of NORIAN is also higher. In conclusion, it is thus reasonable to assume that the homogeneous distribution of the porosity and the lower density of the apatite network between the granules favor a faster *in vivo* degradation of the HBS cement, thus explaining the higher bone substitution properties evidenced in this study. Hence, although showing larger pores, the mineral density around the preferential paths in NORIAN is very high thereby leading to a slower resorption rate.

5. Conclusion

The purpose of this study was to compare the physical and biological properties of two injectable apatitic calcium phosphate cements used in clinics which rely on two different concepts for creating porosity in the CPC once hardened: (i) one purely inorganic CPC (NORIAN) containing calcium carbonate whose degradation results in the creation of porosity through the release of carbon dioxide; (ii) one organic-inorganic formulation (HBS) for which porosity is created thanks to the presence of a cellulose ether which swells in the intergranular space, thus creating channels in the cement microstructure. Percolation of a 0.9 wt.% sodium chloride aqueous solution and titriated water through molded hardened cement blocks showed that both CPCs have comparable permeability but that the water-accessible porosity is far lower than the total porosity measured by mercury intrusion, thus giving evidence of preferential paths for water penetration. However, the biological behavior of the two cements was found to be significantly different, when implanted in critical-sized defects created in the distal lateral femoral condyle of rats. Indeed, the quantitative histomorphometrical analysis of bone explants revealed a significantly higher bone area density at all implantation times in the case of HBS by comparison with NORIAN, as well as a significantly lower cement area density after 8 and 12 weeks of implantation. The arrangement of the apatite crystals in the intergranular space of hardened cements may account for this difference, i.e. a densely packed arrangement of apatite crystals, as observed for NORIAN, would result in an enhancement of the mechanical strength of the CPC but would also slow down its *in vivo* resorption. This suggests that when designing an injectable CPC, a compromise has to be found between its mechanical properties and the kinetics of its *in vivo* degradation.

6. Disclosure

Some authors of this publication have research support from Graftys SA. The terms of this arrangement have been reviewed and approved by both CNRS and the University of Nantes in

accordance with their policy on objectivity in research.

Acknowledgements

This research was carried out with a financial support of Graftys SA. The support of Eric Chevrel from the DSEE laboratory (Hg porosity measurements) and Paul Pilet is greatly acknowledged.

References

1. Brown WE, Chow LC. A new calcium phosphate setting cement. J Dent Res 1983;62:672-679.
2. LeGeros R, Chohayeb A, Shulman A. Apatitic calcium phosphates: possible restorative materials. J Dent Res 1982;61 (Special Issue):343.
3. Mirtchi AA, Lemaitre J, Terao N. Calcium-phosphate cements - study of the beta-tricalcium phosphate - monocalcium phosphate system. Biomaterials 1989;10:475-480.
4. Bajammal SS, Zlowodzki M, Lelwica A, et al. The use of calcium phosphate bone cement in fracture treatment. J Bone Joint Surg Am 2008;90A:1186-1196.
5. Carey LE, Xu HHK, Simon CG, Takagi S, Chow LC. Premixed rapid-setting calcium phosphate composites for bone repair. Biomaterials 2005;26:5002-5014.
6. Larsson S, Bauer TW. Use of injectable calcium phosphate cement for fracture fixation: A review. Clin Orthop Relat Res 2002:23-32.
7. Larsson S, Hannink G. Injectable bone-graft substitutes: Current products, their characteristics and indications, and new developments. Injury 2011;42:S30-S34.
8. Bohner M, Gbureck U, Barralet JE. Technological issues for the development of more efficient calcium phosphate bone cements: A critical assessment. Biomaterials 2005;26:6423-6429.
9. Dorozhkin SV. Calcium orthophosphate cements for biomedical application. J Mater Sci 2008;43:3028-3057.
10. Dorozhkin SV. Self-setting calcium orthophosphate formulations. J Funct Biomater 2013;4:209-311.
11. Ginebra MP, Espanol M, Montufar EB, Perez RA, Mestres G. New processing approaches in calcium phosphate cements and their applications in regenerative medicine. Acta Biomater 2010;6:2863-2873.
12. Khairoun I, Magne D, Gauthier O, et al. In vitro characterization and in vivo properties of a carbonated apatite bone cement. J Biomed Mater Res 2002;60:633-642.
13. Bohner M, Baroud G. Injectability of calcium phosphate pastes. Biomaterials 2005;26:1553.
14. Habib M, Baroud G, Gitzhofer F, Bohner M. Mechanisms underlying the limited injectability of hydraulic calcium phosphate paste. Acta Biomater 2008;4:1465-1471.

15. Khairoun I, Boltong MG, Driessens FCM, Planell JA. Some factors controlling the injectability of calcium phosphate bone cements. J Mater Sci Mater Med 1998;9:425-428.
16. O'Neill R, McCarthy HO, Montufar EB, et al. Critical review: Injectability of calcium phosphate pastes and cements. Acta Biomater 2017;50:1-19.
17. Bohner M, Doebelin N, Baroud G. Theoretical and experimental approach to test the cohesion of calcium phosphate pastes. Eur Cells Mater 2006;12:26-35.
18. Chen G, Li W, Yu X, Sun K. Study of the cohesion of TTCP/DCPA phosphate cement through evolution of cohesion time and remaining percentage. J Mater Sci 2009;44:828-834.
19. Fernandez E, Gil FJ, Best SM, Ginebra MP, Driessens FCM, Planell JA. Improvement of the mechanical properties of new calcium phosphate bone cements in the CaHPO4-alpha-Ca-3(PO4)(2) system: Compressive strength and microstructural development. J Biomed Mater Res 1998;41:560-567.
20. Johnson AJW, Herschler BA. A review of the mechanical behavior of CaP and CaP/polymer composites for applications in bone replacement and repair. Acta Biomater 2011;7:16-30.
21. Zhang J, Liu W, Schnitzler V, Tancret F, Bouler J-M. Calcium phosphate cements for bone substitution: Chemistry, handling and mechanical properties. Acta Biomater 2014;10:1035-1049.
22. Zhang JT, Tancret F, Bouler JM. Fabrication and mechanical properties of calcium phosphate cements (CPC) for bone substitution. Mater Sci Eng C Mater Biol Appl 2011;31:740-747.
23. del Real RP, Ooms E, Wolke JGC, Vallet-Regi M, Jansen JA. In vivo bone response to porous calcium phosphate cement. J Biomed Mater Res Part A 2003;65A:30-36.
24. Gauthier O, Bouler JM, Aguado E, Pilet P, Daculsi G. Macroporous biphasic calcium phosphate ceramics: influence of macropore diameter and macroporosity percentage on bone ingrowth. Biomaterials 1998;19:133-139.
25. Xu HHK, Takagi S, Quinn JB, Chow LC. Fast-setting calcium phosphate scaffolds with tailored macropore formation rates for bone regeneration. J Biomed Mater Res Part A 2004;68A:725-734.
26. Alkhraisat MH, Rueda C, Marino FT, et al. The effect of hyaluronic acid on brushite cement cohesion. Acta Biomater 2009;5:3150-3156.
27. Ishikawa K, Miyamoto Y, Kon M, Nagayama M, Asaoka K. Non-decay type fast-setting calcium-phosphate cement - composite with sodium alginate. Biomaterials 1995;16:527-532.
28. Lin JP, Zhang SN, Chen T, Liu CS, Lin SL, Tian XH. Calcium phosphate cement reinforced by polypeptide copolymers. J Biomed Mater Res Part B 2006;76B:432-439.
29. Liu H, Li H, Cheng WJ, Yang Y, Zhu MY, Zhou CR. Novel injectable calcium phosphate/chitosan composites for bone substitute materials. Acta Biomater 2006;2:557-565.
30. Liu W, Zhang J, Rethore G, et al. A novel injectable, cohesive and toughened Si-HPMC (silanized-hydroxypropyl methylcellulose) composite calcium phosphate cement for bone substitution. Acta Biomater 2014;10:3335-3345.
31. Liu W, Zhang J, Weiss P, Tancret F, Bouler J-M. The influence of different cellulose ethers on both the handling and mechanical properties of calcium phosphate cements for bone substitution. Acta Biomater 2013;9:5740-5750.
32. Miyamoto Y, Ishikawa K, Takechi M, et al. Basic properties of calcium phosphate cement containing atelocollagen in its liquid or powder phases. Biomaterials 1998;19:707-715.
33. Tajima S, Nishimoto N, Kishi Y, Matsuya S, Ishikawa K. Effects of added sodium alginate on mechanical strength of apatite cement. Dent Mater J 2004;23:329-334.
34. Takagi S, Chow LC, Hirayama S, Eichmiller FC. Properties of elastomeric calcium phosphate cement-chitosan composites. Dent Mater 2003;19:797-804.
35. Xu HHK, Simon CG. Fast setting calcium phosphate-chitosan scaffold: mechanical

properties and biocompatibility. Biomaterials 2005;26:1337-1348.
36. Zhang J, Liu W, Gauthier O, et al. A simple and effective approach to prepare injectable macroporous calcium phosphate cement for bone repair: Syringe-foaming using a viscous hydrophilic polymeric solution. Acta Biomater 2016;31:326-338.
37. Burguera EF, Xu HHK, Weir MD. Injectable and rapid-setting calcium phosphate bone cement with dicalcium phosphate dihydrate. J Biomed Mater Res Part B 2006;77B:126-134.
38. Cherng A, Takagi S, Chow LC. Effects of hydroxypropyl methylcellulose and other gelling agents on the handling properties of calcium phosphate cement. J Biomed Mater Res 1997;35:273-277.
39. Jyoti MA, Thai VV, Min YK, Lee B-T, Song H-Y. In vitro bioactivity and biocompatibility of calcium phosphate cements using Hydroxy-propyl-methyl-Cellulose (HPMC). Appl Surf Sci 2010;257:1533-1539.
40. Khairoun I, Driessens FCM, Boltong MG, Planell JA, Wenz R. Addition of cohesion promoters to calcium phosphate cements. Biomaterials 1999;20:393-398.
41. Song H-Y, Rahman AHME, Lee B-T. Fabrication of calcium phosphate-calcium sulfate injectable bone substitute using chitosan and citric acid. J Mater Sci Mater Med 2009;20:935-941.
42. Thai VV, Lee B-T. Fabrication of calcium phosphate-calcium sulfate injectable bone substitute using hydroxy-propyl-methyl-cellulose and citric acid. J Mater Sci Mater Med 2010;21:1867-1874.
43. Wang X, Chen L, Xiang H, Ye J. Influence of anti-washout agents on the rheological properties and injectability of a calcium phosphate cement. J Biomed Mater Res Part B 2007;81B:410-418.
44. Khayat KH. Viscosity-enhancing admixtures for cement-based materials - An overview. Cement Concrete Comp 1998;20:171-188.
45. Patural L, Marchal P, Govin A, Grosseau P, Ruot B, Deves O. Cellulose ethers influence on water retention and consistency in cement-based mortars. Cem Concr Res 2011;41:46-55.
46. Pourchez J, Peschard A, Grosseau P, Guyonnet R, Guilhot B, Vallee F. HPMC and HEMC influence on cement hydration. Cem Concr Res 2006;36:288-294.
47. Mahaguna V, Talbert RL, Peters JI, et al. Influence of hydroxypropyl methylcellulose polymer on in vitro and in vivo performance of controlled release tablets containing alprazolam. Eur J Pharm Biopharm 2003;56:461-468.
48. Siepmann J, Peppas NA. Modeling of drug release from delivery systems based on hydroxypropyl methylcellulose (HPMC). Adv Drug Deliv Rev 2001;48:139-157.
49. Laib S, Fellah BH, Fatimi A, et al. The in vivo degradation of a ruthenium labelled polysaccharide-based hydrogel for bone tissue engineering. Biomaterials 2009;30:1568-1577.
50. Rozema FR, Bergsma JE, Bos RRM, et al. Late degradation simulation of poly(L-lactide). J Mater Sci Mater Med 1994;5:575-581.
51. Graftys. https://clinicaltrialsgov/ct2/show/study/NCT02575352.
52. Ollivier M, Gay AM, Cerlier A, Lunebourg A, Argenson JN, Parratte S. Can we achieve bone healing using the diamond concept without bone grafting for recalcitrant tibial nonunions? Injury 2015;46:1383-1388.
53. Ollivier M, Turati M, Munier M, Lunebourg A, Argenson J-N, Parratte S. Balloon tibioplasty for reduction of depressed tibial plateau fractures: Preliminary radiographic and clinical results. Int Orthop 2016;40:1961-1966.
54. Young AA, Neyton L, Molony DC, Boileau P, Walch G. Glenoid Tricortical Iliac Crest Structural Bone Graft Enhanced With Resorbable Cement for the Treatment ofAseptic Glenoid Loosening. Tech Shoulder Elb Surg 2011;12:12-17.
55. Dupleichs M, Masson M, Gauthier O, et al. Pain management after bone reconstruction surgery using an analgesic bone cement: a functional noninvasive in vivo study using gait

analysis. J Pain 2018;19:1169-1180.
56. Le Ferrec M, Mellier C, Boukhechba F, et al. Design and properties of a novel radiopaque injectable apatitic calcium phosphate cement, suitable for image-guided implantation. J Biomed Mater Res Part B 2018;106:2786-2795.

Table 1. Experimental data related to the permeability, porosity, density and compressive strength of the investigated cements.

Cement sample	HBS	HBS-0	NORIAN
Volume of the percolated sample (cm^3)	20±1	2.4±0.1	2.1±0.1
Permeability ($m\ s^{-1}$)[a]	10^{-8}	5×10^{-11}	6×10^{-8}
Water-accessible porosity (%)	4.9±0.5[b]	63±6[c]	9±1[b]
Total porosity measured by Hg intrusion (%)	61±6	53±5	44±4
Apparent density measured by Hg intrusion ($g.cm^{-3}$)	0.99±0.01	1.16±0.01	1.16±0.01
Porosity measured by gravimetry (%)	63±3	52±3	47±2
Compressive strength (MPa)	13±3	15±3	33±3

[a]Due to the small volume of the cement samples, the precision of the given value is one order of magnitude. [b]Flow rate: 10 μL min^{-1}. [c]Pressure at the column inlet: 40 bars.

Table 2. Histomorphometrical results of the Cement area density (%) and Bone area density (%) in the ROI 2, as a function of the implantation period (*= $p<0.05$ compared to the NORIAN cement).

	HBS		**NORIAN**	
Implantation time	Cement area density (%)	Bone area density (%)	Cement area density (%)	Bone area density (%)
4 weeks	88.6 ± 13.2	5.6 ± 1.7*	99.0 ± 0.9	0.6 ± 0.2
8 weeks	76.9 ± 15.5*	13.5 ± 4.1*	98.9 ± 0.9	0.8 ± 0.2
12 weeks	79.1 ± 15.7*	11.0 ± 3.3*	97.5± 0.9	1.5 ± 0.5

Figure 1: Regions of Interest (ROI) investigated for the histomorphometrical analysis.

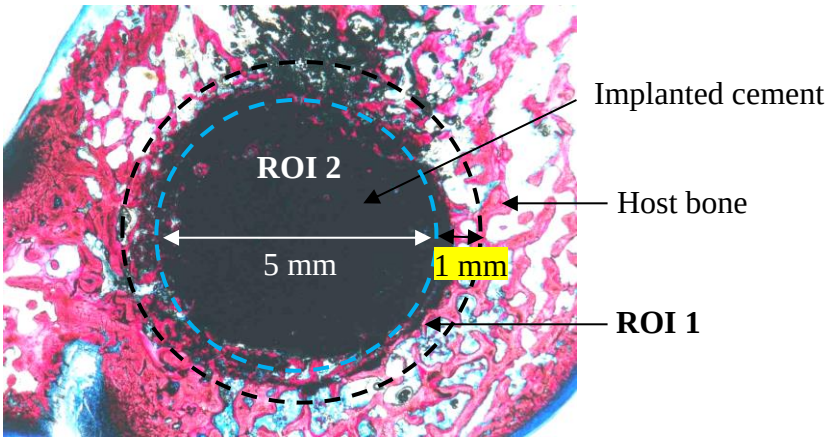

Figure 2. Compared XRD patterns (top view) and FTIR spectra (bottom view) of HBS and NORIAN samples after a setting time of 1 week.

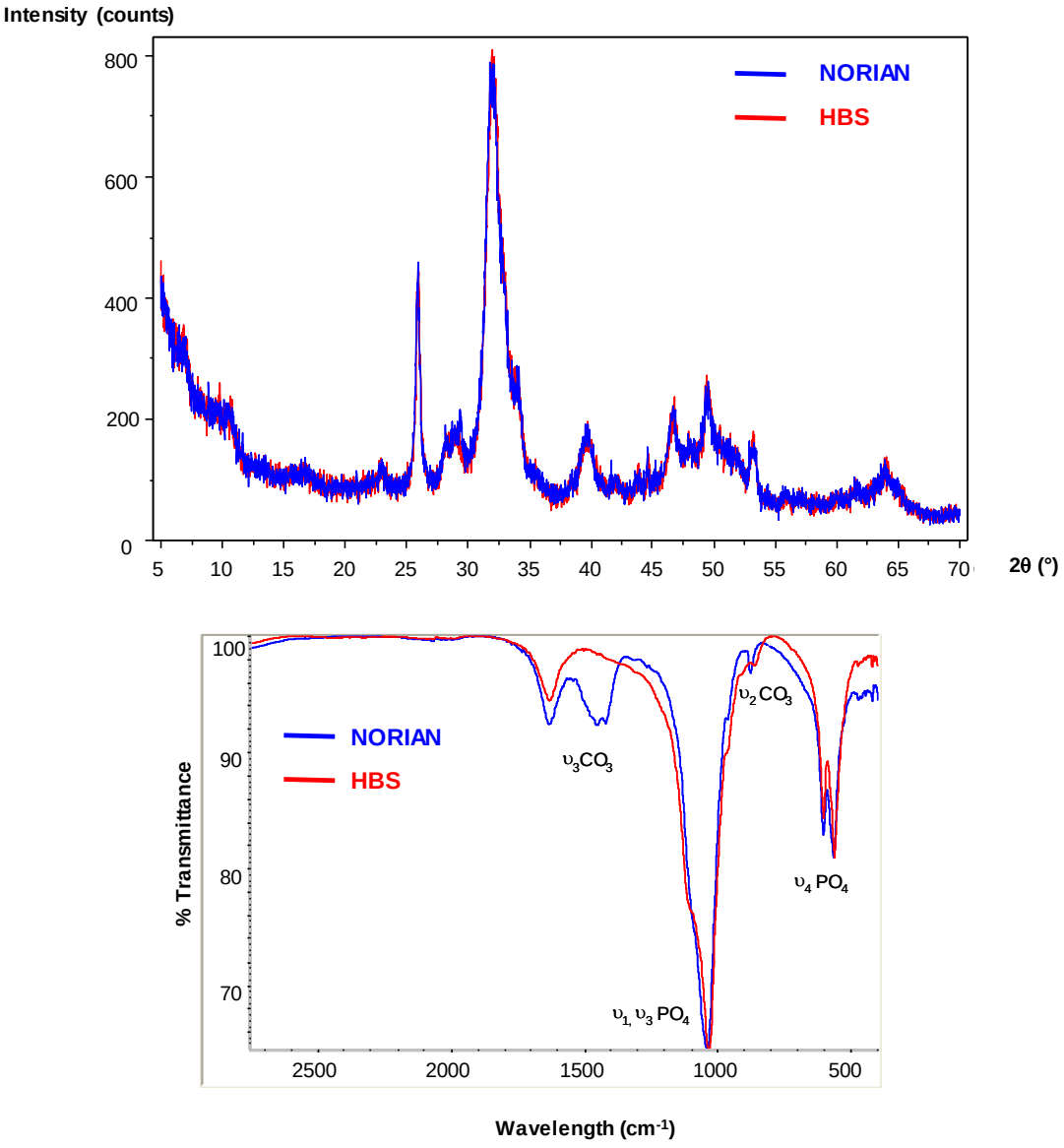

Figure 3. SEM observation of percolated HBS (left views) and HBS-0 (right views) samples (setting time: 1 week): polished cross-section for a ×1800 (top views) and ×4000 magnification (middle views); fracture plane for a ×5000 magnification (bottom views).

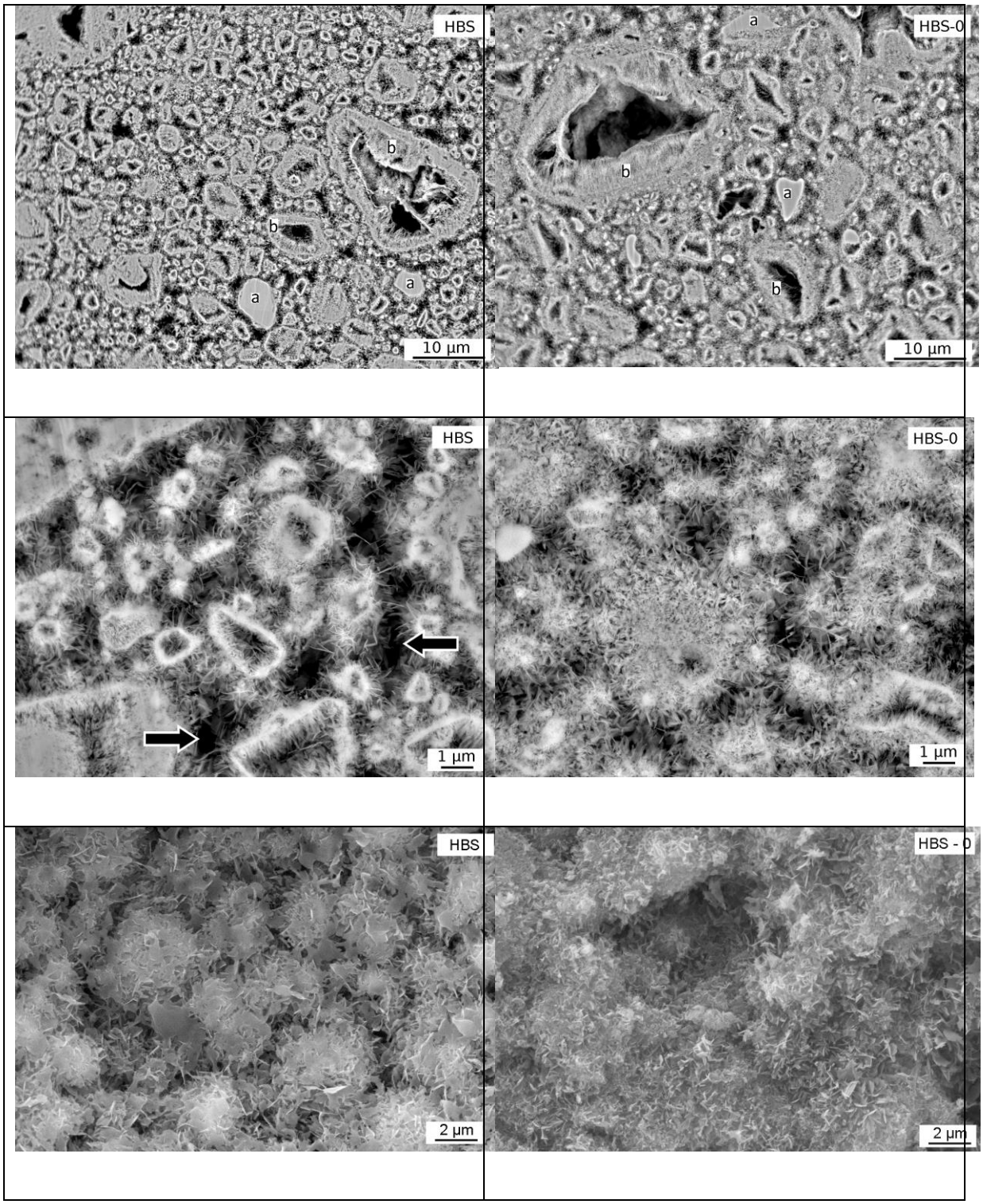

Figure 4. SEM observation of a percolated NORIAN sample (setting time: 1 week): polished cross-section for a ×1800 (left top view) and ×4000 magnification (right top view); fracture plane for a ×5000 magnification (bottom view).

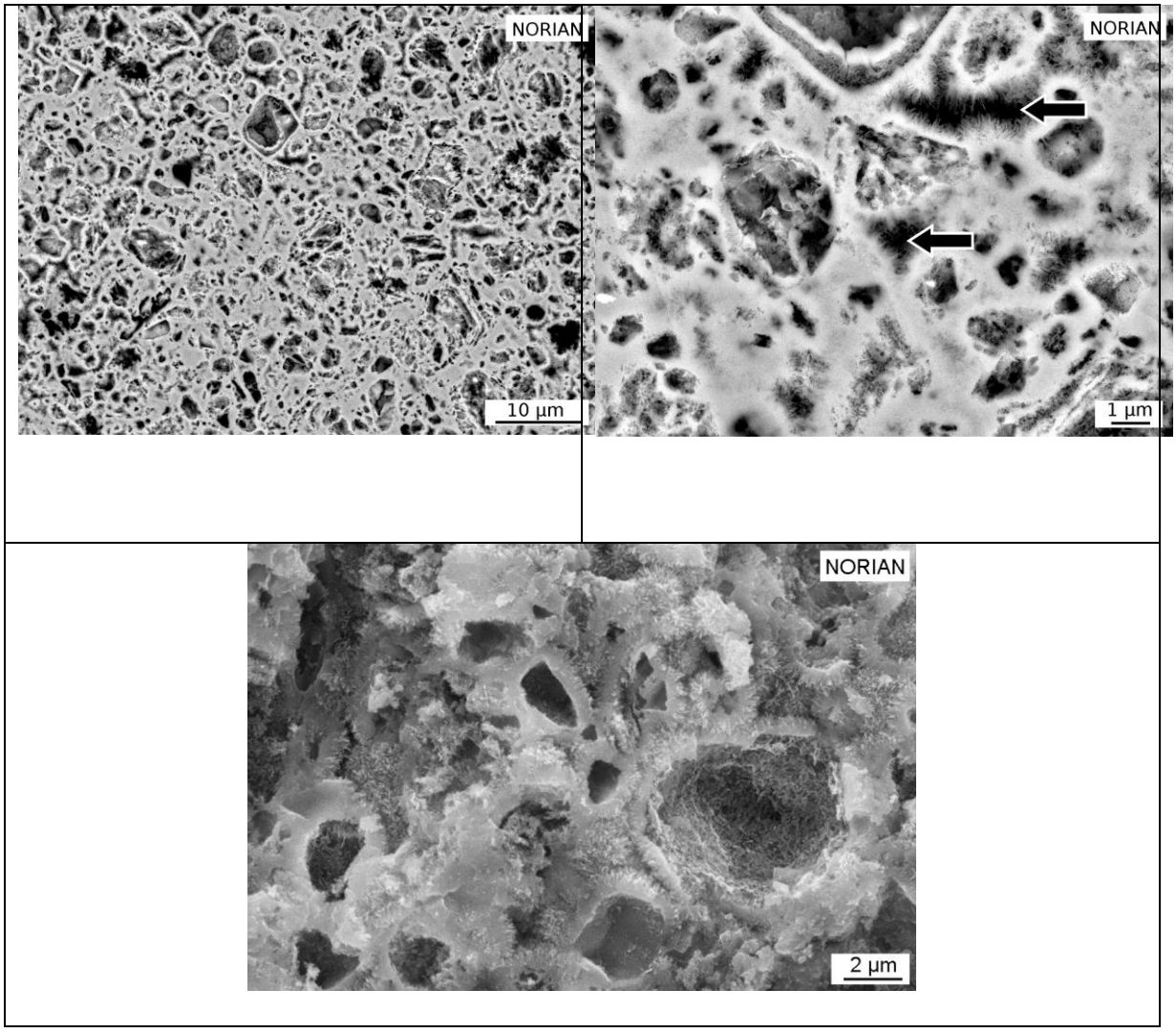

Figure 5. SEM images (×35 magnification) of (a1-a2) NORIAN and (b1-b2) HBS after 8 weeks of implantation: a1 and b1 (respectively a2 and b2) correspond to the same animal that was implanted with HBS on one side and NORIAN on the other side. The remaining cements appear in light grey, while the new and host bone in darker grey. Some new bone formation was observed inside the HBS cement and in the fractured areas of the NORIAN cement. The amount of degradation of the two cements was significantly different, with HBS exhibiting more abundant degradation than NORIAN in both ROI.

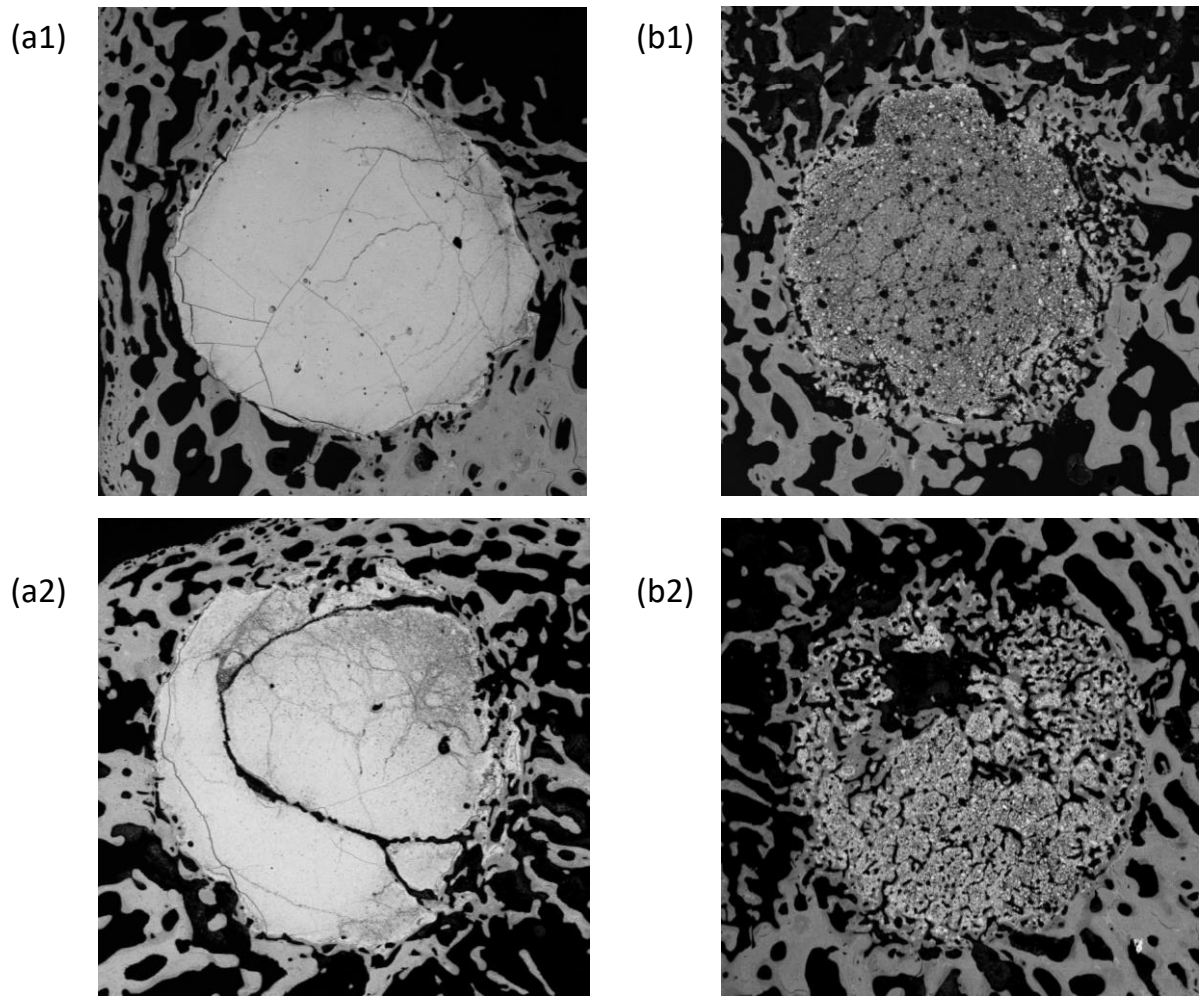

Supporting Information

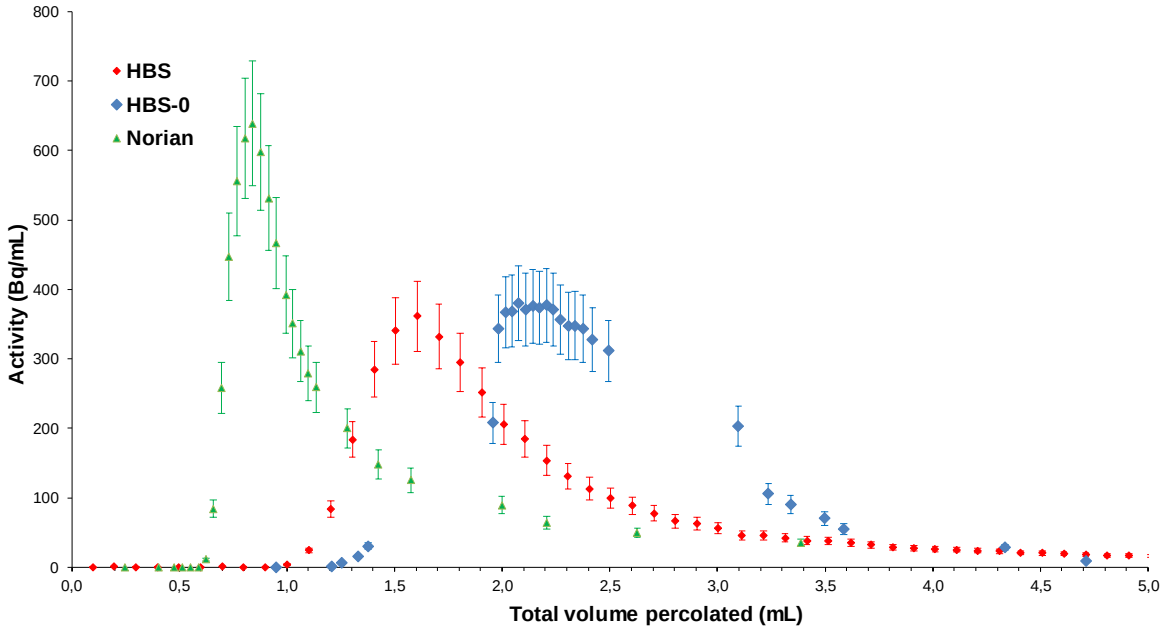

Figure S1. Elution profile of tritiated water injected and percolated through the Norian (green triangles), HBS (red diamonds) and HBS-0 (blue diamonds) samples, under a 0.9 wt.% sodium chloride aqueous solution flow. The water-accessible porosity was calculated as (Vmax – Vd) × 100 / Vc, where Vmax is the eluted volume at the maximum of the ^{3}H detection, Vd is the dead volume of the column, and Vc is the volume of the cement sample.

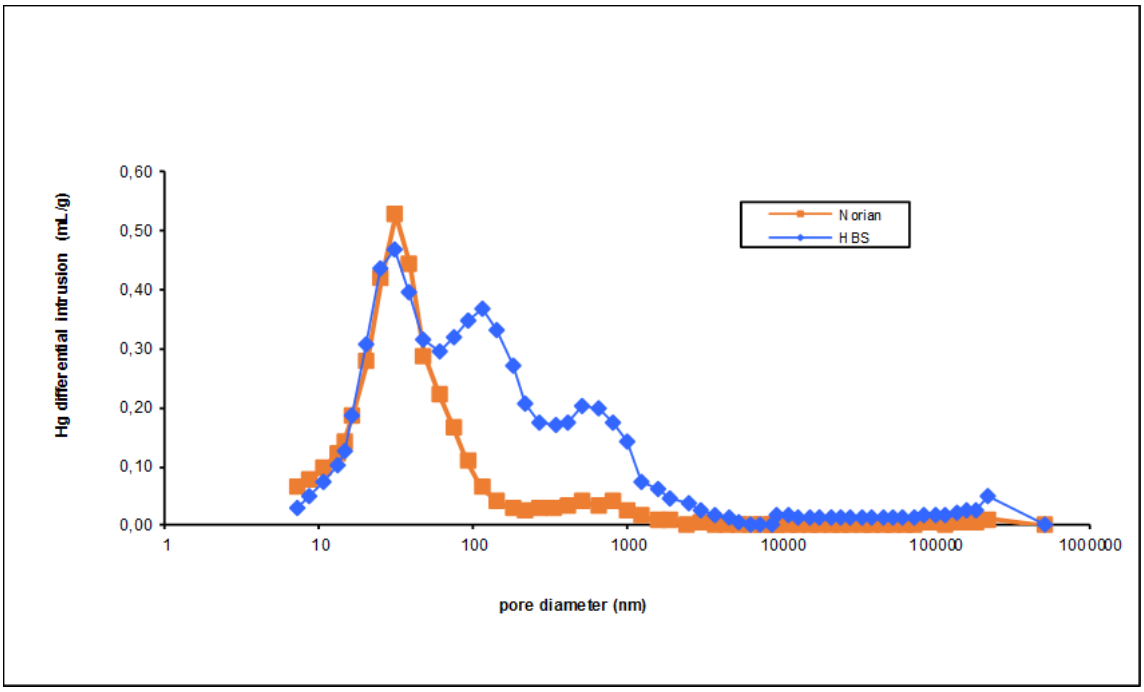

Figure S2. Differential mercury intrusion curves, as a function of the pore size, for the Norian (orange squares) and HBS (blue diamonds) samples

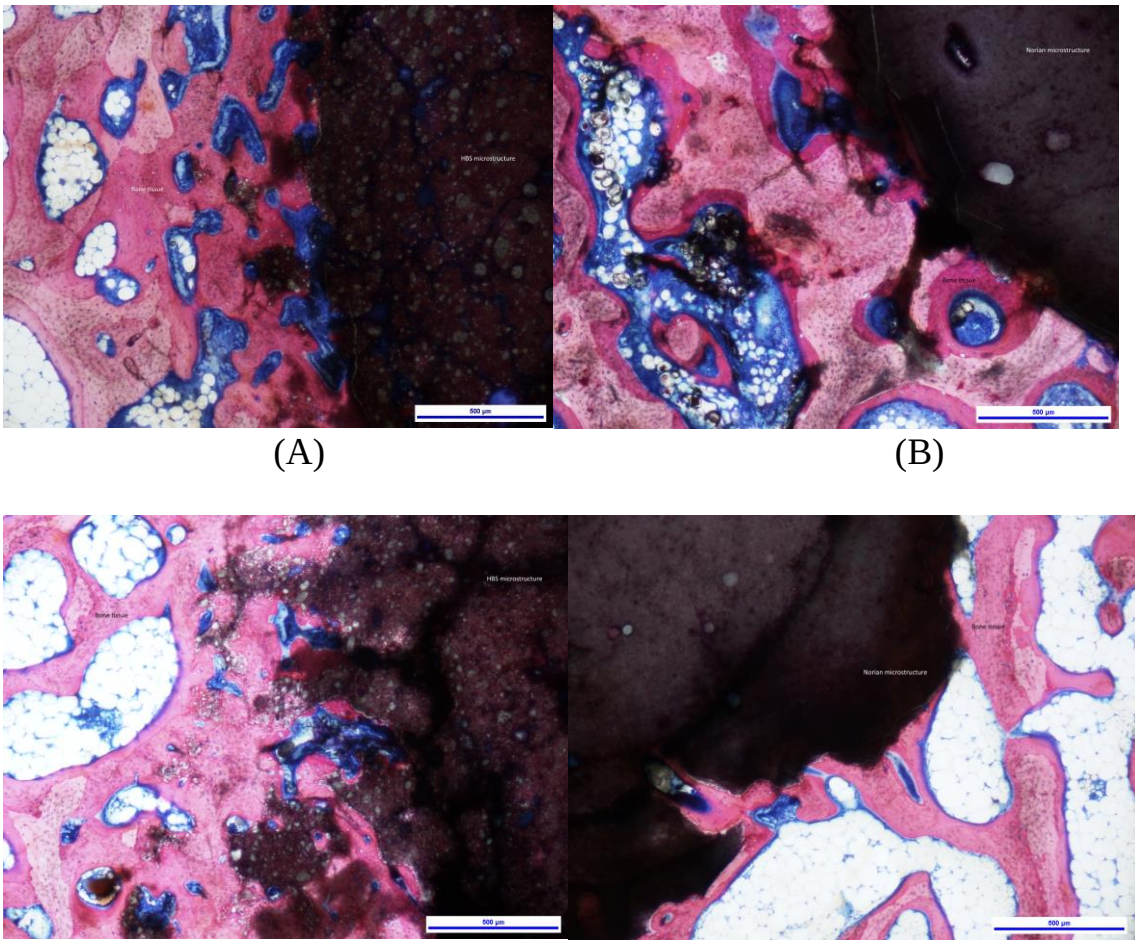

(A) (B)

(C) (D)

Figure S3. Histological sections of stained explants from rabbits implanted with HBS (implantation time: 8 weeks (A) and 12 weeks (C)) or Norian (implantation time: 8weeks (B) and 12 weeks (D)). *The cements appear in grey / dark grey*.